The Planetary Science Journal, 2:102 (12pp), 2021 June https://doi.org/10.3847/PSJ/abf490

Silicon and Oxygen Isotope Evolution of the Inner Solar System

Ryoji Tanaka, Christian Potiszil, and Eizo Nakamura
The Pheasant Memorial Laboratory for Geochemistry and Cosmochemistry, Institute for Planetary Materials, Okayama University, Misasa, Tottori, 682-0193, Japan
ryoji@misasa.okayama-u.ac.jp
Received 2020 August 13; revised 2021 March 17; accepted 2021 March 31; published 2021 May 20

Abstract

Enstatite chondrites have been regarded as major building blocks of the Earth and other differentiated inner planetary bodies due to the similarity of $\Delta^{17}O$ (deviation of the $\delta^{17}O$ value from the terrestrial silicate fractionation line) and nucleosynthetic isotope anomalies. However, this hypothesis has been rebutted by the fact that the Earth and enstatite chondrites show distinct Si isotopic compositions. It has been debated whether the origin of this Si isotope difference is the result of nebular or planetary processes. Here we show that the $\delta^{30}Si$ (deviation of $^{30}Si/^{28}Si$ relative to NBS 28 standard) and the $\Delta^{17}O$ values of chondrules in unequilibrated enstatite chondrites are between −0.20‰ and −0.54‰ and −0.36‰ and +0.26‰, respectively. Furthermore, the chondrules with higher $\Delta^{17}O$ values tend to have lower $\delta^{30}Si$. The data exhibit values consistent with most of the noncarbonaceous group differentiated planetary bodies. This consistency suggests that the Si and O isotopic compositions of enstatite chondrules record those of the major precursors that formed the differentiated planetary bodies in the inner solar system. Model calculations based on the results reveal that the Si and O isotope variations of the enstatite chondrite chondrules were generated by an interaction between the evaporation-driven SiO-rich gas and partially or fully melted forsterite-rich precursor chondrules. The Mg/Si of the evaporated dust-gas mixtures increased with increasing silicate/metal ratio in the evaporated dust, which may have increased the bulk Mg/Si and $\delta^{30}Si$ value of the inner planetary bodies.

Unified Astronomy Thesaurus concepts: Protoplanetary disks (1300); Solar system terrestrial planets (797); Chondrites (228); Chondrules (229); Cosmochemistry (331)

1. Introduction

The isotopic compositions of meteorites and their components have provided essential information for understanding the origin and evolution of inner planetary bodies. Nucleosynthetic isotope anomalies of neutron-rich isotopes (e.g., ^{48}Ca, ^{50}Ti, ^{54}Cr, ^{62}Ni, and r-process Mo) distinguish classes of meteorites into noncarbonaceous (NC) and carbonaceous (CC) groups (Trinquier et al. 2007; Warren 2011; Budde et al. 2016). The NC-CC dichotomy indicates the presence of heterogeneity between presolar materials inside and outside the molecular cloud, which is thought to form the isotopic differences in the meteorite parent bodies (Kleine et al. 2020). The ordinary and enstatite chondrites, Earth, Moon, Mars, and most of the achondrites (e.g., ureilites, angrites, HEDs, and acapulcoites) are classified into the NC group. Variations in the nucleosynthetic isotopes of lithophile elements (^{48}Ca, ^{50}Ti, and ^{54}Cr), from the NC group differentiated planetary bodies, are positively correlated with their parent planetary body's mass, which can be used as a proxy for the planetary body's accretionary timescale (Schiller et al. 2018). This correlation suggests that the material that formed the inner planets was the result of mixing between the early (0.1Ma after CAI) inner solar system material depleted in ^{48}Ca, ^{50}Ti, and ^{54}Cr and that represented by ureilite and the CC group materials enriched in ^{48}Ca, ^{50}Ti, and ^{54}Cr (Schiller et al. 2018). Although the aforementioned nucleosynthetic isotope tracers have revealed the relationship between nebular heterogeneity and the source materials of the inner planetary bodies, the total mass fraction of Ca, Ti, and Cr in the inner planetary bodies is only a few weight percent (Trønnes et al. 2019). Therefore it is crucial to examine whether the isotopic variations of the major elements in rocky planetary materials are consistent with planet formation models predicted by nucleosynthetic anomalies.

Silicon and O account for about half of the mass of inner planetary bodies and represent significant components within the disk; both solid and gas-phase materials could have strongly influenced the Si and O isotopic compositions of the inner planetary bodies. The O isotopic composition in meteorites is mainly characterized by mass-independent isotopic variations, expressed as a $\Delta^{17}O$ value that represents their deviation from the terrestrial silicate fractionation line (definition is given in the footnote of Table 1). Variations in the $\Delta^{17}O$ values of planetary materials were broadly attributed to the mixing of ^{16}O-rich and ^{16}O-poor reservoirs that could have resulted from photochemical reactions (Clayton 2002). Although the timing and location of the photochemical reactions that formed the ^{16}O-rich and ^{16}O-poor reservoirs is still unknown, these reactions could have occurred in the parent molecular cloud from which the solar system formed (Krot et al. 2020). The nucleosynthetic isotope anomalies of ^{48}Ca, ^{50}Ti, ^{54}Cr, and ^{64}Ni correlate well with $\Delta^{17}O$ values in CC meteorites, indicating a genetic relationship (Trinquier et al. 2007; Yin et al. 2009; Dauphas & Schauble 2016). On the other hand, the $\Delta^{17}O$ values of NC meteorites do not correlate with ^{48}Ca, ^{50}Ti, ^{54}Cr, and ^{64}Ni. Furthermore, because the range in $\Delta^{17}O$ values of NC meteorites, except for ordinary chondrites and R (Rumurti) chondrites, overlaps with that of CC meteorites, it has recently been argued that the $\Delta^{17}O$ values should not be included in the definition of the NC-CC dichotomy (Kleine et al. 2020). Thus, it is likely that the $\Delta^{17}O$ values of the source materials that formed the NC meteorite parent bodies may not be directly related to the nucleosynthetic

Table 1
Silicon and Oxygen Isotopic Compositions (±2SE) of Enstatite Chondrite Chondrules and Monomict Ureilites

Sample (type)	Fraction[a]	weight (mg)[b]	δ^{29}Si (‰)		δ^{30}Si (‰)		N[c]	δ^{18}O (‰)		δ^{17}O (‰)		Δ^{17}O (‰)[d]	
Enstatite chondrite chondrule and enstatite fraction													
Sahara 97103	Ch1	0.42	−0.106	±0.017	−0.267	±0.040	4	5.845	±0.006[e]	3.072	±0.013[e]	0.029	±0.026[e]
(EH3)	En1	0.59	−0.242	±0.021	−0.436	±0.022	5	5.989	±0.004[e]	3.152	±0.009[e]	0.034	±0.018[e]
Y-691 (EH3)	Ch comp2	0.49	−0.194	±0.014	−0.404	±0.024	4	5.683	±0.004[e]	2.678	±0.009[e]	−0.279	±0.019[e]
	Ch comp5	0.52	−0.210	±0.014	−0.303	±0.021	8	5.594	±0.006[e]	2.630	±0.011[e]	−0.280	±0.026[e]
Indarch (EH4)	Ch1	0.50	−0.267	±0.020	−0.487	±0.020	8	5.637	±0.005[e]	3.035	±0.006[e]	0.101	±0.013[e]
	Ch comp1	0.79	−0.262	±0.026	−0.510	±0.010	4	5.762	±0.004[e]	2.927	±0.010[e]	−0.073	±0.019[e]
	Ch21	0.29	−0.224	±0.032	−0.443	±0.014	4	5.745	±0.005	3.249	±0.008	0.258	±0.016
	Ch23	0.13	−0.237	±0.015	−0.452	±0.046	4	5.314	±0.004	2.874	±0.008	0.110	±0.016
	Ch25	0.32	−0.249	±0.020	−0.432	±0.030	4	5.460	±0.004	2.960	±0.008	0.119	±0.017
Y-74370 (EH4)	Ch5	0.34	−0.129	±0.022	−0.202	±0.033	8	5.232	±0.005[e]	2.365	±0.010[e]	−0.355	±0.020[e]
	Ch comp1	0.67	−0.166	±0.022	−0.325	±0.016	5	5.255	±0.005[e]	2.452	±0.003[e]	−0.280	±0.007[e]
Y-791810 (EH4)	Ch5	0.34	−0.311	±0.026	−0.521	±0.021	4	5.773	±0.007[e]	3.121	±0.014[e]	0.115	±0.029[e]
	Ch comp1	0.75	−0.286	±0.026	−0.540	±0.013	5	5.772	±0.003	3.179	±0.008	0.174	±0.016
St. Mark's (EH5)	Ch comp1	0.96	−0.299	±0.012	−0.572	±0.019	5	5.476	±0.006[e]	2.839	±0.007[e]	−0.010	±0.017[e]
Y-980223 (EH6)	En1	0.70	−0.275	±0.012	−0.496	±0.023	4	5.866	±0.004[e]	3.201	±0.011[e]	0.146	±0.023[e]
Ureilite													
DaG 340		0.89	−0.247	±0.019	−0.430	±0.022	4	7.529	±0.038	2.742	±0.034	−1.182	±0.024
DaG 868		0.97	−0.216	±0.005	−0.447	±0.027	3	7.804	±0.016	2.973	±0.017	−1.095	±0.017
Dho 132		1.00	−0.240	±0.016	−0.449	±0.023	4	6.764	±0.009	1.942	±0.018	−1.579	±0.021
Dho 836		0.93	−0.222	±0.013	−0.436	±0.023	4	8.096	±0.024	3.444	±0.018	−0.778	±0.019
El Gouanem		0.94	−0.253	±0.011	−0.447	±0.022	3	7.928	±0.010	3.067	±0.021	−1.066	±0.020
NWA 766		1.18	−0.231	±0.015	−0.433	±0.042	4	8.088	±0.012	3.463	±0.016	−0.755	±0.017
NWA 1241		0.90	−0.221	±0.009	−0.434	±0.017	3	7.479	±0.011	2.615	±0.021	−1.283	±0.021
NWA 2376		1.04	−0.230	±0.015	−0.504	±0.017	4						
duplicate		3.06	−0.226	±0.003	−0.499	±0.017	3						
average			−0.228		−0.502			8.276	±0.040	3.313	±0.029	−1.003	±0.027
Y-791538		1.06	−0.223	±0.007	−0.509	±0.013	6						
duplicate		0.98	−0.231	±0.017	−0.503	±0.017	4						
average			−0.227		−0.506			5.646	±0.001	1.044	±0.008	−1.891	±0.008
Y-980110		1.12	−0.233	±0.030	−0.461	±0.029	3	7.853	±0.035	3.137	±0.030	−0.957	±0.011
Y-981688		1.07	−0.225	±0.015	−0.461	±0.014	4	8.157	±0.015	3.385	±0.005	−0.869	±0.013
Y-981750		1.08	−0.227	±0.006	−0.467	±0.040	4	7.396	±0.097	2.867	±0.058	−0.988	±0.007
Y-982143		0.97	−0.214	±0.016	−0.420	±0.021	3	7.497	±0.152	2.877	±0.070	−1.031	±0.009
A-880784		0.93	−0.234	±0.007	−0.433	±0.022	3						
duplicate		1.01	−0.249	±0.008	−0.430	±0.021	3						
average			−0.242		−0.432			6.015	±0.033	0.946	±0.010	−2.182	±0.008
Nova 018		0.92	−0.215	±0.006	−0.404	±0.019	3	8.580	±0.002	4.160	±0.008	−0.319	±0.007
Ureilite average (±2SD)			−0.229	±0.023	−0.449	±0.055							

Notes.
[a] For single chondrules, the split ones were used for the O and Si isotope analysis, respectively (shown as Ch*). Chondrule composites (Ch comp*) and enstatite fractions (En*) were ground in a mortar and pestle, and the fractions were split for the O and Si isotope analysis.
[b] Weight: weight of the sample for the Si isotope measurement
[c] N: number of Si isotope measurements per samples.
[d] $\Delta^{17}O = \delta^{17}O' - 0.527 \times \delta^{18}O'$, where $\delta^{17}O' = \ln(\delta^{17}O^* + 1)$, $\delta^{17}O^* = \delta^{17}O + 0.039 \times 10^{-3}$, and $\delta^{18}O' = \ln(\delta^{18}O + 1)$.
[e] Data are from Tanaka & Nakamura (2017).

isotope anomalies in their source materials. The Δ^{17}O values in NC achondrites could be related to a kinetic process operating in the inner disk, such as a solid-gas reaction (Tanaka & Nakamura 2017).

For Si isotopes, no resolvable mass-independent variation of Si isotopes was found in bulk meteorites and their components, except for presolar grains, suggesting that Si isotopic homogenization was achieved in the solar nebula prior to planetary accretion (Pringle et al. 2013b). The δ^{30}Si values, which express the Si isotope composition of the sample relative to that of the NBS 28 standard, $\delta^{30}Si = [(^{30}Si/^{28}Si)_{sample}/(^{30}Si/^{28}Si)_{NBS28} - 1]$, for carbonaceous and ordinary chondrites, show the same value (-0.47 ± 0.07‰, 2SD, $N = 34$), which is referred to as the chondritic value (Figure 1). In contrast, many NC group planetary materials, i.e., enstatite chondrites (ECs), HEDs, angrites, aubrites, bulk silicate Earth (BSE), and the Moon, show variable values that differ from the chondritic value (Figure 1). The cause of the mass-dependent Si isotopic variations of NC group planetary materials have been discussed in terms of either nebular or planetary processes (e.g., Georg et al. 2007; Fitoussi et al. 2009; Savage et al. 2010, 2014; Armytage et al. 2011, 2012; Fitoussi & Bourdon 2012; Pringle et al. 2013a, 2013b; Savage & Moynier 2013; Zambardi et al. 2013; Dauphas et al. 2015; Young et al. 2019; Sikdar & Rai 2020). However, little research has been done to explore the causes of Si isotope variations of NC group planetary bodies in terms of the relationship with O isotopes (e.g., Hin et al. 2017).

Elucidating the isotope systematics of Si and O in the NC group can provide essential information for deciphering the

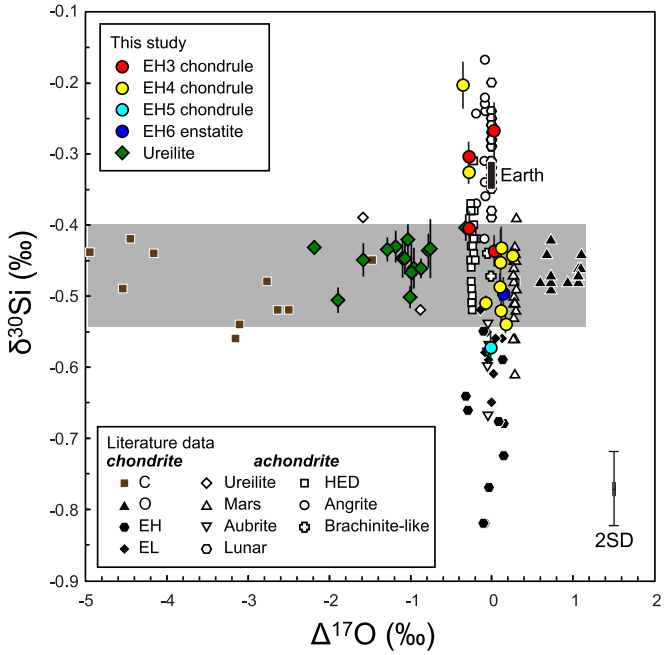

Figure 1. The $\Delta^{17}O$ values vs. $\delta^{30}Si$ values of enstatite chondrite chondrules and ureilite plotted with other meteorite groups. C indicates carbonaceous chondrite (CC group) and O ordinary chondrite (NC group). EH and EL chondrites and all achondrites belong to the NC group. The error bar for each data point is two standard errors. The 2SD external precision of the reference materials is shown in the bottom right corner. The gray zone indicates the range of $\Delta^{17}O$ values and the 2SD range of $\delta^{30}Si$ values of carbonaceous and ordinary chondrites. The $\Delta^{17}O$ and $\delta^{30}Si$ values of the literature data are from Ali et al. (2016), Armytage et al. (2011, 2012), Clayton et al. (1991), Dauphas et al. (2015), Defouilloy et al. (2016), Fitoussi & Bourdon (2012), Fitoussi et al. (2009, 2016), Franchi et al. (1999), Georg et al. (2007), Greenwood et al. (2017), Newton et al. (2000), Patzer & Schultz (2001), Pringle et al. (2014), Pringle et al. (2013a), Sikdar & Rai (2020), Savage et al. (2014, 2010), Savage & Moynier (2013), Wiechert et al. (2004), and Zambardi et al. (2013). Lunar samples whose $\Delta^{17}O$ values were not measured are fixed as $\Delta^{17}O = 0$. The $\Delta^{17}O$ values for H, L, and LL ordinary chondrites whose values were not measured were fixed as the average value of H, L, and LL (Greenwood et al. 2012), respectively.

evolution of the inner planetary body precursors during nebular evolution, including condensation, evaporation, and gas-solid interactions. The bulk isotopic composition of meteorites reflects the average composition of the precursor materials in the region where each meteorite parent body was accreted. Planetary processes could have partially or entirely homogenized the initial isotopic heterogeneity of the precursor materials. Therefore it is necessary to measure the isotopic variability of primitive components in chondrites in order to decipher the evolution of the precursors of inner planetary bodies in more detail. Chondrules are millimeter-sized, silicate-rich spheres that formed from fully or partially molten droplets in protoplanetary disks. Chondrules, along with matrix phases, which are thought to form complementarily from the same reservoir (Palme et al. 2015), are the major components of chondrites. Furthermore, chondrules are regarded as the main building blocks of planetesimals and planetary embryos (Johansen et al. 2015). Thus, the chemical and isotopic composition of chondrules provides essential information for understanding the origin and evolution of the inner planets.

Enstatite chondrites possess O and nucleosynthetic isotope values that are the most similar within the chondrite group to those of the Earth and Moon and are thus considered the main building blocks of these planetary bodies. Chondrules in ECs have $\Delta^{17}O$ values identical to the NC group differentiated asteroids, indicating that the formation of EC chondrules is closely related to the precursors of inner planets (Tanaka & Nakamura 2017). On the other hand, Si isotopes in enstatite chondrites and the related achondrites, aubrites, have distinctly lower $\delta^{30}Si$ values than the other NC group planetary bodies. The low $\delta^{30}Si$ values of these enstatite meteorites were assumed to result from the presence of metallic phases with low $\delta^{30}Si$ values (Savage & Moynier 2013; Kadlag et al. 2019; Sikdar & Rai 2020). In contrast, silicate fractions in ECs extend from chondritic to heavier than the chondritic values (Ziegler et al. 2010; Armytage et al. 2011; Fitoussi & Bourdon 2012; Savage & Moynier 2013; Kadlag et al. 2019; Sikdar & Rai 2020). There is no evidence for diffusive re-equilibration of Si isotopes between silicate and metal phases in EH3 and EH4 chondrites (Kadlag et al. 2019). Therefore the metal and silicate phases of ECs were assumed to have condensed from or reacted with nebular gases with different $\delta^{30}Si$ values (Sikdar & Rai 2020), but the cause of this Si isotope heterogeneity has not been well explained.

Ureilites are ultramafic achondrites predominantly composed of olivine and pyroxene and are generally interpreted as originating from the mantle of a partially differentiated parent body, the ureilite parent body (Scott et al. 1993). As mentioned previously, ureilites are found at one end of a nucleosynthetic isotope anomaly line (depleted in ^{48}Ca, ^{50}Ti, and ^{54}Cr) and thus represent the members of the NC group that are least affected by the CC component. The O isotopic compositions of ureilites are plotted on or near the carbonaceous chondritic anhydrous mineral (CCAM) line (Clayton & Mayeda 1988; Figure 2). This O isotope coincidence is considered crucial evidence that ureilites inherited the isotopic compositions of nebular precursors present in the early inner solar disk material that was not significantly modified by later planetary processes (Clayton & Mayeda 1988). Therefore the Si-O isotope systematics of ureilites likely record that of the early, that is, <0.1 Myr after the formation of CAIs, inner solar disk material. The $\delta^{30}Si$ values of ureilites were previously measured for only four samples, -0.47 ± 0.12‰; 2SD, and were found to be identical to the chondritic value (Armytage et al. 2011). However, the relationship of $\delta^{30}Si$ with O isotopes has not been examined.

Here we report the Si and O isotopic compositions of the chondrules in EH chondrites. The EL chondrites were not studied here because their primary compositions may have been modified by impact process (Weisberg & Kimura 2012). As a supplemental data set, the Si and O isotopic compositions of ureilites that have an extensive range of $\Delta^{17}O$ values are also reported. Based on the obtained results and previously reported data, we elucidate the process responsible for Si–O isotope evolution in the inner solar system and discuss its implications for the formation processes that yield the inner planetary bodies.

2. Samples and Experimental Techniques

Chondrules and enstatite fractions separated from seven EH chondrites were analyzed in this study: Sahara 97103 (EH3), Yamato 691 (Y-691, EH3), Indarch (EH4), Yamato 74370 (Y-74370, EH4), Yamato 791810 (Y-791810, EH4), St. Mark's (NHMW_#6536_B, EH5), and Yamato 980223 (Y-980223, EH6). Most of the samples analyzed were already separated for O isotope analysis (Tanaka & Nakamura 2017), and the remaining fractions were used in this study for the Si isotope

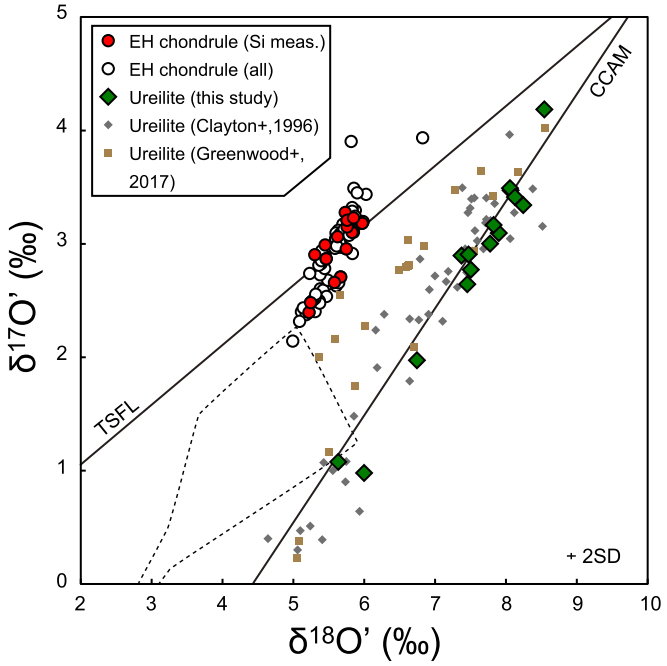

Figure 2. Oxygen isotopic compositions of EC chondrules and ureilites. Red circles are data for EH3 and EH4 chondrules presented in Table 1. Open circles are all data for EH3 and EH4 chondrules and enstatite separates measured elsewhere (Tanaka & Nakamura 2017) whose Si isotopic compositions were not measured. The compiled data of ureilites are from Clayton & Mayeda (1996) and Greenwood et al. (2017). TSFL is the terrestrial silicate fractionation line (Tanaka & Nakamura 2017), and CCAM is the carbonaceous chondritic anhydrous mineral line (Clayton & Mayeda 1988). The range for chondrules and isolated olivine in carbonaceous chondrites (Clayton et al. 1983; Rubin et al. 1990; Russell et al. 2010) is shown with a broken line.

analysis. Additional chondrule fractions were also separated from Y-791810 and Indarch using a method described elsewhere (Tanaka & Nakamura 2017). The analyzed chondrules show either porphyritic pyroxene or radial pyroxene textures. The main constituent mineral of the representative samples was enstatite (Mg# = 0.98–1.00, defined as mole fraction Mg/[Mg+Fe]) with and without anhedral relict forsterite (Mg# = 0.99–1.00) associated with a minor amount of albitic glass/plagioclase and mesostasis and with an accessory amount of Ca-rich pyroxene, troilite, niningerite, and daubreelite.

For the ureilites, 15 monomict meteorites (DaG 340, DaG 868, Dho 132, Dho 836, El Gouanem, NWA 766, NWA 1241, NWA 2376, Y-791538, Y-980110, Y-981688, Y-981750, Y-982143, A-880784, and Nova 018) were selected for analysis. All of the ureilite samples are partially weathered. As the pristine O and Si isotopic compositions can be altered by weathering processes (Newton et al. 2000; Ziegler et al. 2005), workup procedures are essential to ensure that any measurements probe the pristine isotopic compositions of the samples. Furthermore, ureilites generally contain a few wt.% of carbon, which results in the production of C–O–F compounds during laser fluorination of silicates. The presence of C–O–F compounds results in a low recovery yield of O_2. We found that the $\delta^{17}O$ and $\delta^{18}O$ values of olivine and pyroxene artificially mixed with carbon gave higher values than the original values even after removing the formed C-O-F compounds and CF_4 from O_2 by the gas chromatographic or cryogenic procedures. Thus, the altered fractions and C-bearing phases were removed before isotope analysis as follows. Chunks of ureilites were crushed using a silicon nitride pestle and mortar, then sieved into 73–200 μm size fractions. After removing magnetic fractions using a ferrite magnet, the remaining fraction was leached in ethanolamine thioglycollate dissolved in isopropanol to remove weathering products, then rinsed with isopropanol (Martins et al. 2007). Magnetic fractions and carbon fractions were further removed using an Nd-magnet and hand-picking under a binocular microscope, respectively. Finally, the samples were washed in deionized water and dried.

The analytical method for determining the Si isotopic composition of the EC chondrules and ureilites from the current study is based on Georg et al. (2006). A mass of 0.1–1 mg of coarse-grained or powdered sample was mixed with ~30 times that weight in NaOH pellets (Merck, EMSURE®) within a 99.9 % silver capsule, put in a cleaned silver crucible with a lid, and then fused at 730°C for 10 minutes in a furnace. After fusing, the silver capsule containing the sample was transferred into a Teflon vial containing 5–20 mL of water and kept in a dark place for 24 hr. The sample solution was then transferred into a polypropylene bottle and rinsed three times with water to ensure maximum recovery. The solution was acidified by adding 2M HNO_3 and water to adjust the pH to between 2.2 and 2.4 and the Si concentration to ~6 μg mL^{-1}. The Si in the sample solution was purified by 1.8 mL of cation exchanged resin (BioRad AG50W-X12, 200–400 mesh), which was packed in a polypropylene column (ID ~7mm, Muromachi Chemical Inc.) and in the H^+ form. The resin was cleaned before sample preparation by passing 10 mL of 6 mol L^{-1} HCl, 10 mL of 8 mol L^{-1} HNO_3, 5 mL of 6 mol L^{-1} HCl, 5 mL of 3 mol L^{-1} HCl, and 6 mL of water. After cleaning the resin, a collection beaker was placed beneath the column. Subsequently, 5 mL of sample solution was loaded onto the resin, followed by 3.8 mL of water to recover Si. The eluted solution was acidified by adding 70 % HNO_3 to 1 % v/v HNO_3 for the analysis. The recovery of Si at the end of the whole procedure was measured using reference materials (NBS-28, IRMM-018a, Big Batch, Diatomite, and BHVO-2) and was found to be >96%.

Silicon isotope measurements were performed on a MC-ICP-MS (Neptune-Plus, Thermo Fisher Scientific) in the high-resolution mode under a wet plasma condition. A sapphire torch, Ni normal sample cone, and Ni-X skimmer cone were used. Typically, 3.0–3.5 μg mL^{-1} of Si dissolved in 1 % v/v HNO_3 were introduced into the plasma via a 50 μL/min self-aspirating PFA microflow nebulizer (Elemental Scientific) and a Peltier-cooled double-pass silica glass cyclonic spray chamber. The isotopes of ^{28}Si, ^{29}Si, and ^{30}Si were measured using Faraday cups L3, C, and H3, respectively, equipped with 10^{11} Ω resistors. The intensities of ^{28}Si for the peak and background signals were usually ~5 V and ~0.03 V, respectively. The Si masses were resolved from the interferences (e.g., $^{12}C^{16}O^+$, $^{14}N_2^+$, $^{28}Si^1H^+$, and $^{14}N^{16}O^+$) on the low-mass side of the Si plateau peak. To correct for instrument mass bias, a standard-sample bracketing method was performed using NBS28 as a bracketing standard. Each measurement consisted of 50 cycles of 4 s integration for the sample and 30 cycles of 4 s integration for the background, and the data outside of 2SD were rejected. More than three measurements were performed for each sample; the average and 2SE of the replicated data are shown in Table 1. Silicon isotope values are defined using the delta notation as

$$\delta^{29\ or\ 30}Si = [(^{29\ or\ 30}Si/^{28}Si_{sample})/(^{29\ or\ 30}Si/^{28}Si_{NBS28}) - 1].$$

The average values and external precisions (2SD) of standards routinely analyzed along with the samples were

$\delta^{29}Si = -0.146 \pm 0.040‰$ and $\delta^{30}Si = -0.292 \pm 0.054‰$ for BHVO-2 ($N = 9$), $\delta^{29}Si = -1.005 \pm 0.020‰$ and $\delta^{30}Si = -1.925 \pm 0.075‰$ for IRMM-018a ($N = 3$), $\delta^{29}Si = 0.644 \pm 0.048‰$ and $\delta^{30}Si = 1.265 \pm 0.058‰$ for Diatomite standard ($N = 9$), and $\delta^{29}Si = -5.484 \pm 0.019‰$ and $\delta^{30}Si = -10.687 \pm 0.051‰$ for Big Batch ($N = 4$). The above values are in good agreement with published values (Reynolds et al. 2007; Savage et al. 2014) except for IRMM-018a (Valkiers et al. 2005), where the data have not yet been characterized by inter-laboratory comparison. The 3σ detection limit defined by the intensity of ^{28}Si from the carrier solution was 0.4 ng mL^{-1}. The total procedural blank, determined by performing the same procedure without adding sample during fusion, was <0.7 ng mL^{-1} in the analyzing solution. The blank fraction in the sample solution was $<\sim 0.02\%$; thus, the blank effect is negligible.

Oxygen isotope measurements were performed using the laser fluorination method. The detailed analytical method is described elsewhere (Tanaka & Nakamura 2013; Pack et al. 2016; Tanaka & Nakamura 2017). The O_2 from the sample was extracted using a CO_2 laser with BrF_5 as an oxidation agent. The extracted O_2 was purified in the extraction line, then trapped with a 13 Å molecular sieve at the temperature of liquid N_2. The isotope ratios in the extracted O_2 gas were determined using a gas-source mass spectrometer (MAT253, Thermo Fisher Scientific) in dual inlet mode. For each sample, eight blocks of 11 cycles each were measured with a total measurement time of ~90 minutes. For the ureilite samples, duplicate measurements were performed, and the average values are shown in Table 1. The working reference gas was calibrated by VSMOW2 and SLAP2, and all data are expressed using the VSMOW2/SLAP2 scale. The $^{18}O/^{16}O$ and $^{17}O/^{16}O$ of the sample is expressed as the common delta notation relative to VSMOW2 as $\delta^{17 \text{ or } 18}O = (^{17 \text{ or } 18}O/^{16}O_{sample})/(^{17 \text{ or } 18}O/^{16}O_{VSMOW2})–1$. Repeat analyses of San Carlos olivine (MSOL-1) determined the analytical uncertainty for the data were performed before and after the analysis of every 2–3 unknowns. The intermediate precision of MSOL-1 was obtained as $\delta^{17}O = 2.737 \pm 0.028‰$, $\delta^{18}O = 5.278 \pm 0.062‰$, and $\Delta^{17}O = -0.002 \pm 0.018‰$ (2SD, $N = 8$).

3. Results

Silicon and O isotopic data for EC chondrules and ureilites are shown in Table 1. Most of the O isotope data for EC chondrules presented here were reported elsewhere (Tanaka & Nakamura 2017), and all the newly analyzed data are within the range of the previously reported data set (Table 1 and Figure 2). The $\delta^{30}Si$ and $\delta^{29}Si$ values fall on a mass-dependent fractionation line of $\delta^{29}Si \sim 0.5 \times \delta^{30}Si$. Thus, only $\delta^{30}Si$ values are discussed in this study. The $\delta^{30}Si$ values of the chondrules range between $-0.57 \pm 0.02‰$ and $-0.20 \pm 0.03‰$ (the error is 2SE, and the same is true thereafter). Most of the $\delta^{30}Si$ values obtained (Figure 1) are either higher than or within the range of the bulk EH ($-0.87‰$ to $-0.51‰$) and EL chondrites ($-0.69‰$ to $-0.49‰$) values, including the 2SE range of the published data).

The $\delta^{30}Si$ and $\Delta^{17}O$ values of EH chondrules do not show a clear correlation (Figure 3). However, with one exception (Sahara 97103 Ch1), they form two clusters: the $\delta^{30}Si$ values of chondrules at $\Delta^{17}O > -0.1‰$ are between $-0.43‰$ and $-0.54‰$, which is identical to the chondritic value, while those with $\Delta^{17}O < -0.2‰$ are between $-0.20‰$ and $-0.40‰$, which is higher than that of the chondritic value. The exception, Sahara 97103 Ch1, has a $\Delta^{17}O$ value in the range of the first cluster (chondritic value) and a $\delta^{30}Si$ value in the range of the second cluster, close to the Earth's composition.

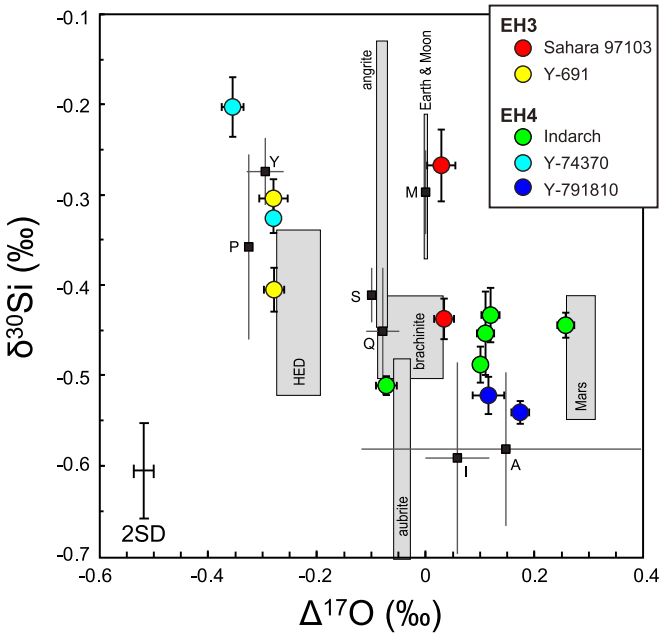

Figure 3. $\Delta^{17}O$ values vs. $\delta^{30}Si$ values of EH3 and EH4 chondrules. The solid square shows $\Delta^{17}O$ values of the bulk composition (Newton et al. 2000; Defouilloy et al. 2016; Tanaka & Nakamura 2017) and $\delta^{30}Si$ values of silicate or nonmagnetic fractions (Ziegler et al. 2010; Fitoussi & Bourdon 2012; Savage & Moynier 2013; Sikdar & Rai 2020) from a different batch of EH3 and EH4 chondrites: A = Abee, I = Indarch, M = MIL 07028, P = PCA 91461, Q = Qingzhen, S = Sahara 97158 and Sahara 97096, and Y = Y-691. The error bars for the bulk data are 2SE. The errors of the $\Delta^{17}O$ values for PCA 91461 and MIL 07028 were not reported in the reference. The $\Delta^{17}O$ value for Y-691 is the average value for chondrules and enstatite fractions (Tanaka & Nakamura 2017). The 2SD range of achondrites, Earth's mantle, and the Moon are also shown. The error bar for each data point is 2 SE. The 2SD external precision of the reference materials is shown in the bottom left corner.

Oxygen isotopic compositions of analyzed chondrules and enstatites in EH5 and EH6 have been partially and fully equilibrated, respectively, on the parent body (Tanaka & Nakamura 2017). The lower $\delta^{30}Si$ values of chondrules in St. Marks, relative to EH3 and EH4 chondrules could have been caused by the partial equilibration between silicate and metal during metamorphism. Therefore data obtained from EH5 and EH6 are not discussed in this study.

The O isotopic composition of the 15 monomict ureilites measured in this study show a range of $\delta^{18}O$ values from 5.6 to 8.6‰ and $\Delta^{17}O$ values from $-2.18‰$ to $-0.32‰$, which all align along the CCAM (Figure 2). The measured $\Delta^{17}O$ range accounts for 84% of the $\Delta^{17}O$ range ($-2.49‰$ to $-0.28‰$) for all the ureilites reported to date (Figure 2). The measured $\delta^{30}Si$ values of these monomict ureilites give a homogeneous value of $-0.449 \pm 0.055‰$ (2SD, $N = 15$), i.e., the 2SD value is comparable with that of reference materials ($\pm 0.054‰$ for BHVO-2; Figure 1). The previously reported Si isotope data (Armytage et al. 2011) are within the range obtained in this study.

4. Discussion

4.1. Silicon and Oxygen Isotopic Characteristics of the EC Chondrule

The heterogeneous $\Delta^{17}O$ values of chondrules from each EH3 and EH4 chondrite demonstrated that they were not

equilibrated in a planetary environment (Tanaka & Nakamura 2017). As the diffusion coefficient of Si in pyroxene is more than one order of magnitude smaller than that of O for a given temperature (Béjina & Jaoul 1996), it is unlikely that the Si isotopic compositions of the measured chondrules in EH3 and EH4 were equilibrated under planetary conditions. Thus, the variation of $\Delta^{17}O$ and $\delta^{30}Si$ values for EH3 and EH4 chondrules (Figure 3) is attributed to the nebular processes. In Figure 3 we also plot the published Si isotopic compositions of silicate or nonmagnetic fractions from each EH3 and EH4 meteorite versus the bulk $\Delta^{17}O$ values of the same meteorite (note that Si and O isotope data were not measured from the same sample batch). The mass fraction of O in the non-silicate fraction, i.e., sulfide and metal, is negligible relative to that in silicate and oxide phases. Thus the relationship between O and Si isotopic data for these compiled data can represent the silicate fraction of these ECs. These compiled data show the same tendency as our data, showing lower $\delta^{30}Si$ values as the $\Delta^{17}O$ value increases in general. Thus, the relationship of Si and O isotopic compositions of both the EC chondrules and the bulk silicates in EC inherits the Si and O isotopic evolution of the nebular processes in the EC chondrule-forming region.

The $\Delta^{17}O$ value of the carbonaceous chondrite chondrules is $-5.5‰$ to $-0.4‰$, which is lower than that of the EC chondrules with one exception (Figure 2). The distinct $\Delta^{17}O$ values of carbonaceous chondrite chondrules and EC chondrules clearly demonstrates that they were formed from different reservoirs. The variation of $\delta^{30}Si$ values of the carbonaceous chondrite chondrules ($-0.86 \pm 0.16‰$ to $+0.33 \pm 0.02‰$; Martins et al. 2021) is larger than that of the EC chondrules. The same is also the case for $\Delta^{17}O$, and the $\delta^{30}Si$ value of the EC chondrules are within the range of CC chondrules. As for the $\delta^{30}Si$ values of the in situ measurements, the carbonaceous chondrite chondrules measured by secondary ion mass spectrometry (SIMS) show a much wider range in values, between $-6.98 \pm 0.36‰$ and $+2.62 \pm 0.31‰$ (Villeneuve et al. 2020), than the bulk chondrule values. On the other hand, the in situ data for EC chondrules measured by laser ablation inductively coupled plasma mass spectrometry (LA-ICP-MS) range from $-1.04 \pm 0.24‰$ to $-0.27 \pm 0.21‰$ (Kadlag et al. 2019), which overlaps with the range of the bulk chondrule and silicate fraction within the analytical uncertainty (2SE), except for one value ($-1.04 \pm 0.24‰$). Although there are differences in the analytical size between SIMS ($\sim 10\,\mu m$) and LA-ICP-MS ($\sim 100\,\mu m$), it is clear that the carbonaceous chondrite chondrules show significantly more heterogeneous $\delta^{30}Si$ values than the EC chondrules. The heterogeneous Si isotopic compositions for carbonaceous chondrite chondrules could be attributed to the precursor's isotopic heterogeneity and kinetic effects during gas-melt interactions (Villeneuve et al. 2020) or nonequilibrium evaporation/condensation processes (Martins et al. 2020) during chondrule formation. The restricted range for $\Delta^{17}O$ and $\delta^{30}Si$ values for EC chondrules indicates that their formation process is different from that of carbonaceous chondrites.

Enstatite chondrite chondrules were formed under a highly reduced nebular environment (Jacquet et al. 2018). The canonical model for EC chondrule formation requires the melting of precursor materials that were condensed from the reduced (e.g., high C/O) region of the solar nebular (Grossman et al. 2008). However, EC components experienced variable redox conditions during their formation (Weisberg et al. 1994). For instance, the presence of titanium valences in olivine and pyroxene from EH3 chondrules suggest that these precursors formed in an environment with an oxygen fugacity close to solar nebula conditions (Simon et al. 2016). The reduced mineralogical features are thought to have been formed by the reaction process of the precursor materials. The frequently preserved relict or poikilitic olivine in low-Ca pyroxene and the presence of silica-containing minerals, which are more common in EC chondrules than in other chondrule clans, is believed to have resulted from the reaction of chondrule precursors and reduced gases. As a reduced gas component, SiO is presumed to be an essential reactant during the crystallization of enstatite from olivine (Libourel et al. 2006). Reactions with S-rich gas, in addition to SiO, could have played an important role in the formation of EC chondrules that contain significant amounts of lithophile element-sulfides and silica minerals (Lehner et al. 2013; Piani et al. 2016). The most dominant mineral in the studied samples is enstatite, with a Mg# that ranges between 0.99 and 1.00, while sulfide minerals are rare and silica minerals are absent. Thus, a SiO-rich gas-melt interaction process should have played an important role in producing the variation of $\delta^{30}Si$ values, as well as the O isotope variations (Tanaka & Nakamura 2017).

4.2. The Silicon and Oxygen Isotopic Characteristics of Ureilites

It is widely accepted that the large range in $\Delta^{17}O$ values for ureilites ($-2‰$ to $0‰$, Figure 2) was inherited from precursor materials that were formed by the mixing of nebular reservoirs, between ^{16}O-rich rocky components and ^{16}O-poor H_2O components (Clayton & Mayeda 1988; Clayton 2002). Thus, the homogeneous Si isotope composition of ureilites, despite the heterogeneous $\Delta^{17}O$ values, suggests that the $\delta^{30}Si$ value of these precursor materials had already reached the homogeneous value of $-0.45‰$ by at least 0.1 My after the formation of the solar system (Schiller et al. 2018). On the other hand, a different hypothesis was proposed in which aqueous alteration by high $\Delta^{17}O$ water/ice within the ureilite parent body was responsible for the heterogeneous $\Delta^{17}O$ values (Sanders et al. 2017). The aqueous alteration hypothesis explained that the $\Delta^{17}O$ values of ureilites should be proportional to the reacted H_2O/silicate ratio (Sanders et al. 2017). Even if the variation of $\Delta^{17}O$ values of the ureilite parent body were due to aqueous alteration, the homogeneous Si isotopic composition implies that the precursor of the ureilite parent body was already homogeneous in its Si isotopic ratio and the system was closed with respect to Si isotopes during low-temperature aqueous alteration. However, the ureilite parent body eventually underwent partial melting, and the Si isotopic ratio should have been fractionated during the processes that occurred prior to this, such as high-temperature hydrothermal alteration and metamorphism. We expect that it is unlikely that all of these planetary process took place under a closed system with respect to Si.

4.3. Silicon and Oxygen Isotope Evolution by the Evaporation-driven Melt-gas Interaction Model

The evaporation-driven melt-gas interaction model was applied to explain the O isotope trend of carbonaceous and

enstatite chondrite chondrules (Marrocchi & Chaussidon 2015; Tanaka & Nakamura 2017). In the current study, the evaporation-driven melt-gas interaction model was applied to EC chondrules, but with the inclusion of Si isotopes in addition to those of O. This model assumes that enstatite-rich chondrules were formed by open-system melt-gas interactions between a precursor forsterite-rich chondrule melt and an evolved SiO-enriched gas that could have occurred over part of the temperature range for chondrule formation. The evolved SiO is a mixture of the initial nebular gas and that from evaporated dust. The Si and O isotopic compositions of the modeled enstatite-rich chondrule were obtained by a mass balance calculation using given values of the precursor chondrule ($\delta^{30}Si_{olivine}$ and $\delta^{17\text{ or }18}O_{olivine}$), initial gas ($\delta^{30}Si_{initial\ gas}$ and $\delta^{17\text{ or }18}O_{initial\ gas}$), dust ($\delta^{30}Si_{dust}$ and $\delta^{17\text{ or }18}O_{dust}$), the dust/gas density ratio (R), and the melt-gas reaction temperature (T).

The molar contents of Si and O and the isotopic compositions of these elements for the evolved gas can be written as

$$[Si]_{gas} = [Si]_{initial\ gas} + R \times [Si]_{dust}, \quad (1)$$

$$[O]_{gas} = [O]_{initial\ gas} + R \times [O]_{dust}, \quad (2)$$

where [Si or O]$_{gas}$, [Si or O]$_{initial\ gas}$, and [Si or O]$_{dust}$ are molar contents of Si or O in the evolved gas, initial gas, and precursor dust, respectively.

Previous studies (Marrocchi & Chaussidon 2015; Tanaka & Nakamura 2017) did not consider the metal phases in the dust component because the O abundance in metallic dust is negligibly low. However, early condensed metal phases under reduced conditions could contain percent levels of the Si mass fraction (Savage & Moynier 2013). The molar contents of Si and O in the silicate dust and metallic dust are expressed as

$$[Si]_{silicate\ dust} = \alpha \times [Si]_{dust}, \quad (3)$$

$$[Si]_{metallic\ dust} = (1 - \alpha) \times [Si]_{dust}, \quad (4)$$

$$[O]_{dust} = [O]_{silicate\ dust}, \quad (5)$$

where $\delta^{30}Si_{silicate\ dust}$ and $\delta^{30}Si_{metallicdust}$ are $\delta^{30}Si$ of silicate dust and metallic dust, respectively, and α is the fraction of [Si]$_{dust}$ from the silicate dust in the metal-silicate dust mixture.

Thus, the Si and O isotopic compositions of dust can be expressed as

$$\delta^{30}Si_{dust} = \alpha \times \delta^{30}Si_{silicate\ dust} + (1 - \alpha) \times \delta^{30}Si_{metallic\ dust}, \quad (6)$$

$$\delta^{i}O_{dust} = \delta^{i}O_{silicate\ dust}, \quad (7)$$

where i is 17 or 18. The Si and O isotopic compositions of the evolved gas, $\delta^{30}Si_{gas}$ and $\delta^{i}O_{gas}$, respectively, are expressed as

$$\boldsymbol{\delta^{30}Si_{gas}} = \frac{\boldsymbol{\delta^{30}Si_{initial\ gas}} \times [Si]_{initial\ gas} + R \times (\boldsymbol{\alpha} \times \boldsymbol{\delta^{30}Si_{silicate\ dust}} + (1 - \boldsymbol{\alpha}) \times \boldsymbol{\delta^{30}Si_{metalic\ dust}}) \times [Si]_{dust}}{[Si]_{gas}} \quad (8)$$

$$\boldsymbol{\delta^{i}O_{gas}} = \frac{\boldsymbol{\delta^{i}O_{initial\ gas}} \times [O]_{initial\ gas} + R \times \boldsymbol{\delta^{i}O_{silicate\ dust}} \times [O]_{dust}}{[O]_{gas}}, \quad (9)$$

where $\delta^{30}Si_{initial\ gas}$ is the $\delta^{30}Si$ of the initial gas and $\delta^{i}O_{initial\ gas}$ and $\delta^{i}O_{silicate\ dust}$ are the $\delta^{i}O$ of the initial gas and silicate dust, respectively.

Carbon monoxide is the most dominant O-bearing molecule in the solar nebula (Prinn 1993). When the R value increases, partial pressure of SiO could have been increased in the nebula, leading to SiO as an important O-bearing molecule in the gas along with CO. The fraction of O carried by SiO in the gas is defined as

$$f_{SiO} = \frac{[SiO]}{[SiO] + [CO]}, \quad (10)$$

where [SiO] and [CO] are molar contents of the gas in SiO and CO, respectively. The O isotopic composition of the evolved gas can be written as

$$\boldsymbol{\delta^{i}O_{gas}} = f_{SiO} \times \boldsymbol{\delta^{i}O_{SiO\ gas}} + (1 - f_{SiO}) \times \delta^{i}O_{CO\ gas} \quad (11)$$

or

$$\delta^{i}O_{SiO\ gas} = \delta^{i}O_{gas} - (1 - f_{SiO}) \times \Delta^{i}O_{CO\text{-}SiO}, \quad (12)$$

where $\Delta^{i}O_{CO\text{-}SiO}$ is the equilibrium isotopic fractionation of $\delta^{17\text{ or }18}O$ between CO and SiO.

As SiO is the dominant Si-bearing gaseous species, the Si isotopic composition of the gas can be written as

$$\delta^{30}Si_{gas} = \delta^{30}Si_{SiO}. \quad (13)$$

The reaction of SiO into the melt and the reaction between olivine and melt can be written as

$$SiO_{(gas)} + \frac{1}{2}O_{2(gas)} = SiO_{2(melt)}, \quad (14)$$

$$Mg_2SiO_{4(olivine)} + SiO_{2(melt)} = Mg_2Si_2O_{6(melt)} = Mg_2Si_2O_{6(pyroxene)}. \quad (15)$$

Hence, the O and Si isotopic compositions of the pyroxene are

$$\delta^{i}O_{pyroxene} = \frac{2}{3}\delta^{i}O_{olivine} + \frac{1}{3}(\Delta^{i}O_{pyroxene\text{-}SiO} + \delta^{i}O_{SiO}), \quad (16)$$

$$\delta^{30}Si_{pyroxene} = \frac{1}{2}\delta^{30}Si_{olivine} + \frac{1}{2}(\Delta^{30}Si_{pyroxene\text{-}SiO} + \delta^{30}Si_{SiO}), \quad (17)$$

where

$$\delta^{i}O_{SiO} = \frac{\delta^{i}O_{\text{initial gas}} \times [O]_{\text{initial gas}} + R \times \delta^{i}O_{\text{silicate dust}} \times [O]_{\text{dust}}}{[O]_{\text{gas}}} - \frac{\Delta^{i}O_{\text{CO-SiO}}}{1 + [SiO]/[CO]}. \quad (18)$$

The model calculation was performed under different given conditions for T, α, and R values. For the calculation, the chemical compositions of the solar nebular condensate (Fedkin & Grossman 2016) and the solar abundance (Lodders 2003) were used for the precursor dust and initial gas compositions, respectively: $[Si]_{dust} = [Si]_{initial\ gas} = 1 \times 10^{6}$, $[O]_{initial\ gas} = 1.41 \times 10^{7}$, $[O]_{dust} = 3.35 \times 10^{6}$, $[C]_{dust} = 0$, and $[C]_{initial\ gas} = 7.08 \times 10^{6}$. The $\Delta^{i}O_{pyroxene\text{-}SiO}$ and $\Delta^{30}Si_{pyroxene\text{-}SiO}$ values were the temperature-dependent fractionation factors (Javoy et al. 2012). CI dust was used as the precursor dust composition (Marrocchi & Chaussidon 2015; Tanaka & Nakamura 2017). Thus, $\delta^{i}O_{initial\ gas}$ and $\delta^{i}O_{olivine}$ values estimated in Tanaka & Nakamura (2017) were recalculated using the solar nebular condensate (Fedkin & Grossman 2016) as the precursor dust composition using the same calculation method as described in Tanaka & Nakamura (2017), resulting in a $\delta^{18}O_{initial\ gas} = 21‰$, $\delta^{17}O_{initial\ gas} = 20‰$, $\delta^{18}O_{olivine} = 3.5‰$, and $\delta^{17}O_{olivine} = 0.1‰$.

4.4. Silicon Isotopic Compositions of the Dust, Gas, and Precursor Chondrule Melt

Forming a chondrule requires an orders of magnitude higher dust-enrichment than for the canonical solar nebular condition (Alexander et al. 2008). Fedkin & Grossman (2016) calculated the pre-accretionary condensate composition relevant to the dust-enriched region of the inner protoplanetary disk from a nebular of a solar composition. The solar nebular condensates, which equilibrated with solar gas from 2000 to 1400 K at 10^{-3} bar, are forsterite, Fe–Ni metal, enstatite, spinel, and liquid Fe-sulfide, and nearly all Fe existed as Fe–Ni metal and Fe-sulfide (Fedkin & Grossman 2016). The oxygen fugacity of dust-enriched system from a nebular of a solar composition decreases with decreasing temperature, reaching ~−4 relative to the iron-wüstite buffer (IW) at ~1400 K (Fedkin & Grossman 2016). To crystallize Fe–Ni metal with Si >1 wt. % and lithophile element-sulfides, the oxygen fugacity has to be <−3 ~ −4 relative to IW (Berthet et al. 2009). The solar nebular condensate includes ~21 wt.% of sulfide minerals (Fedkin & Grossman 2016). Because sulfide minerals do not contain nominal Si and O, the abundance of sulfide dust were not considered for the calculation. Thus the actual dust/gas ratio should be higher than the calculated R value. Although the abundance of sulfide minerals does not affect the calculation, the evaporation of sulfide dust plays an important role in reducing the system by forming S-rich gas, even for a high dust/gas ratio at 1000 in the solar nebular (Fedkin & Grossman 2016).

The major early phases, which condensed from the solar nebula gas in the innermost region of the protoplanetary disk, include amoeboid olivine aggregates (AOA), CAIs, forsterite, and Fe–Ni metal (Davis & Richter 2014; Scott & Krot 2014). CAIs, the earliest condensates from the cooling solar nebula, have an extensive range of mass-dependent heavy Si isotope enrichments (the $\delta^{30}Si$ can be as high as value up to 14.3‰), revealing kinetic isotope fractionation caused by evaporation (Clayton et al. 1988). Thus, the $\delta^{30}Si$ values of CAIs do not record equilibration with the nebular gas. On the contrary, AOAs were affected by only minor thermal processing after their formation (Scott & Krot 2014). Thus, the forsterites in AOAs preserve the earliest O and Si isotopic compositions of forsterite condensates from the solar nebula, giving $\Delta^{17}O$ of ~−25‰ to −20‰ (Krot et al. 2004) and $\delta^{30}Si$ of −5.2‰ to −2.8‰ (the average $\delta^{30}Si$ values calculated by the multiple in situ data in each AOA of Marrocchi et al. 2019). The $\delta^{30}Si$ value of Fe–Ni metal phases in the EH3 chondrites range between −8.2‰ and −4.0‰ (Kadlag et al. 2019; Sikdar & Rai 2020). Equilibrium fractionation factors of $\delta^{30}Si$ values for forsterite-SiO and $Fe_{1.5}Si$–SiO at 1600 K, i.e., the forsterite and Fe–Ni metal crystallization temperature (Fedkin & Grossman 2016), are +1.67‰ and −0.66‰, respectively (Javoy et al. 2012; Meheut & Schauble 2014). The values obtained for $\delta^{30}Si_{dust}$ are a mixture of the $\delta^{30}Si$ values for silicate minerals and Fe–Ni metal. Thus, various $\delta^{30}Si_{dust}$ values, calculated for different F_{sil} values (a fraction of silicates in a silicate + metal mixture calculated as the weight fraction converted from the α value), were applied in calculations. For the calculation, the Si mass fractions in silicate dust and metallic dust are fixed as 23.7 wt.% and 3 wt.% (Savage & Moynier 2013; Fedkin & Grossman 2016), and the $\delta^{30}Si$ values for silicate dust and metallic dust are fixed as the heaviest value of −0.45‰ and the lowest value of −8.2‰, respectively. Thus, the F_{sil} is a semi-quantitative value.

The $\delta^{30}Si$ values of SiO gas, which equilibrated with forsterite in AOA and Si-bearing Fe–Ni metal calculated at 1600 K, demonstrate overlapping values between −6.8‰ and −4.5‰ and between −7.5‰ and −3.3‰, respectively (Figure 4). The $\delta^{30}Si$ value of SiO, which was equilibrated with the early (i.e., <0.1 Ma after the birth of the solar system) stage bulk inner disk silicates presumed by ureilite, is ~−2‰ to −3‰ (Figure 4). Thus, the $\delta^{30}Si$ values of SiO in the nebula evolved from ~−8‰ to ~−2‰ during condensation of Fe–Ni metal and olivine (Figure 4). The $\delta^{30}Si_{initial\ gas}$ value is fixed as −2.63 and was calculated for SiO gas of a solar composition equilibrated with $\delta^{30}Si_{olivine} = -0.45‰$ at 1400 K (Javoy et al. 2012; Meheut & Schauble 2014; the temperature being just below the condensation temperatures of Fe–Ni metal and forsterite) and at a total pressure of 10^{-3} atm (Davis & Richter 2014).

The $\delta^{30}Si$ of the olivine-rich precursor chondrule melt, expressed by the $\delta^{30}Si_{olivine}$ value, was estimated by the $\delta^{30}Si$ value of the inner planetary disk silicate components represented by ureilites and chondritic value. The O isotopic compositions of ureilites reveal that the inner disk materials had heterogeneous $\Delta^{17}O$ values between −2‰ and 0‰ (Figure 2), which partly overlap with those of chondrules and isolated olivine grains in carbonaceous chondrites ranging between −6‰ and −1‰ (Clayton et al. 1983; Russell et al. 2010). It is a matter of debate whether the carbonaceous chondrite chondrules that formed in the inner solar system subsequently migrated beyond Jupiter's orbit or in the outer solar system (van Kooten et al. 2016). However, the identical $\delta^{30}Si$ values for the ureilite and carbonaceous chondrites

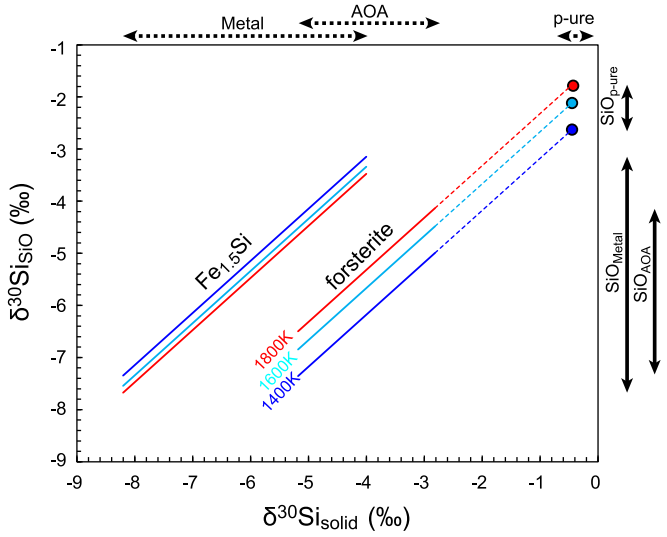

Figure 4. Relationship between δ^{30}Si values of the solid phases ($\delta^{30}Si_{solid}$) and the equilibrated SiO gas ($\delta^{30}Si_{SiO}$). Blue, light blue, and red lines are equilibrium δ^{30}Si values between forsterite and SiO and $Fe_{1.5}Si$ and SiO at 1400, 1600, and 1800 K, respectively. Blue, light blue, and red circles are δ^{30}Si values of SiO that could have equilibrated with ureilite precursors and forsterite-rich chondrule at 1400, 1600, and 1800 K, respectively. The range of δ^{30}Si values of metal, olivine in AOA (the range of average values of in situ data from each AOA of Marrocchi et al. 2019), and the precursor of the ureilite parent body (p-ure) and of SiO equilibrated with metal (SiO_{Metal}), olivine in AOA (SiO_{AOA}), and p-ure (SiO_{p-ure}) are shown with broken and solid lines, respectively.

implies that the Si isotopic compositions of the major disk materials had not been modified by the thermal process in which the nucleosynthetic isotope compositions were modified by selective destruction of presolar components (Trinquier et al. 2009). Thus, the $\delta^{30}Si_{olivine}$ value is fixed at $-0.45‰$ for the calculation.

4.5. Result of the Model Calculations

The calculation was first performed using the fixed F_{sil} values (=0.80) based on the chemical composition of solar condensates (Fedkin & Grossman 2016) and a variable dust/gas density ratio (R) and melt-gas reaction temperature (T) (Figures 5(a), (b)). Figure 5(a) indicates the formation of EC chondrules at R between 3 and 6 and T between 2000 and 2800 K. The Δ^{17}O value of enstatite depends on R but not on T. On the other hand, the δ^{30}Si value of enstatite depends both on T and R values. The Mg/Si atomic ratio of the dust-gas mixture depends on the Δ^{17}O value, namely, the R value at constant F_{sil} value. The silica-rich chondrule in EH4 experienced >1960 K during its cooling process (Tanaka & Nakamura 2017). Thus, T could have been reached at ~2000 K in the chondrule-forming region. However, a T >~2200 K, higher than the liquidus temperature of forsterite, is too high to preserve the relict olivine in the reacted enstatite. The estimated T at ~2000 K is within the range of the chondrule peak temperature (1700–2100 K; Hewins & Connolly 1996). The similar mineralogy of the measured chondrules, mainly showing the porphyritic texture and the common presence of relict olivine, suggests no significant differences in melting temperature and cooling rate for each chondrule. Therefore it is unlikely that the Δ^{17}O–δ^{30}Si variation was mainly attributed to the significant variation of T.

Second, the O and Si isotope variation of pyroxene formed at constant T and variable F_{sil} values were examined (Figures 5(c) and (d)). This condition assumes that the silicate-metal ratio in the condensed dust-gas system had variable proportions due to fractionation of these phases during or after solar gas condensation. The representative figure calculated at $T = 2000$ K is shown in Figures 5(c) and (d). The variation of the δ^{30}Si value is sensitive to the F_{sil} value, the δ^{30}Si value increases with increasing F_{sil} value, while the Δ^{17}O value is less sensitive to the F_{sil} value at a given R value (Figures 5(c) and (d)). The Mg/Si atomic ratio of the dust-gas mixture depends on both the R and F_{sil} values. Figure 5(c) shows that the melt-gas interaction explains why the variation in the Δ^{17}O and δ^{30}Si values of EC chondrules at different dust-gas abundances has variable R and F_{sil} values. One cluster with $\Delta^{17}O < -0.2‰$ is accompanied by the higher R, relatively higher but variable F_{sil} values, and the higher Mg/Si ratio of the dust-gas mixture relative to the other cluster with $\Delta^{17}O > -0.1‰$ (Figure 5(c)). The exception, Sahara 97103 Ch1, can be generated under relatively higher F_{sil} that resemble the former, but a lower R that resembles the latter during melt-gas reaction in the higher Mg/Si ratio of the dust-gas mixture. When the given T increases, the relationship between R and F_{sil} values (red mesh) and Mg/Si (broken blue curves) moves parallel to the y-axis (δ^{30}Si value) and toward higher values, as shown in Figure 5(c). As discussed in the previous paragraph, the thermal history was not significantly different among the measured chondrules. Thus, the preferred explanation, for the cause of the Δ^{17}O and δ^{30}Si variations of EC chondrules, is the variable R and F_{sil} values in the reacted dust-gas environment. Thus, in the environment where the EC chondrules formed, there were regions with relatively high and low levels of dust/gas, silicate/metal in the dust, and Mg/Si in the dust-gas mixtures, which may have determined the variation in the Δ^{17}O and δ^{30}Si values of EC chondrules and the silicate fractions of EC. However, the presence of data outside of these clusters, one chondrule in Sahara 97103 and the silicate fraction of MIL 07028 (Figure 3), suggests that more variable compositional ranges may actually have prevailed.

The matrix of EH3 consists of fine-grained silicate and opaque (Fe–Ni metal and sulfides) minerals (Kimura 1988), and nearly half of the clastic matrix in the EH3 is inferred to be composed of primitive nebular components (Kimura 1988; Rubin et al. 2009). Although the detailed silicate-metal ratio in the primitive nebular components has not been measured, the fine-grained nebular components are composed of various silicate and metal mixtures characterized by heavier and lighter Si isotopic compositions, respectively (Rubin et al. 2009; Sikdar & Rai 2020). These primitive nebular components could be the remnants of the dust components in the EC chondrule-forming region.

The supra-chondritic δ^{30}Si values for silicate fraction in EC were explained by metal-silicate fractionation or vaporization (Sikdar & Rai 2020). However, these equilibrium or kinetic processes cannot fractionate the Δ^{17}O values, as observed in a positive correlation between $\delta^{18}O'$ and $\delta^{17}O'$ with a steep slope of 1.27 for EC chondrules (Figures 5(b) and (d); Tanaka & Nakamura 2017). The subchondritic δ^{30}Si values for silicate fractions reported from two EH4 (Indarch and Abee in Figure 3) cannot be explained by either metal-silicate fractionation or vaporization processes from the chondritic or ureilitic δ^{30}Si source. The bulk Δ^{17}O values of these two chondrites are relatively higher among the EC (Figure 4), indicating that these low δ^{30}Si and high Δ^{17}O values can consistently be explained

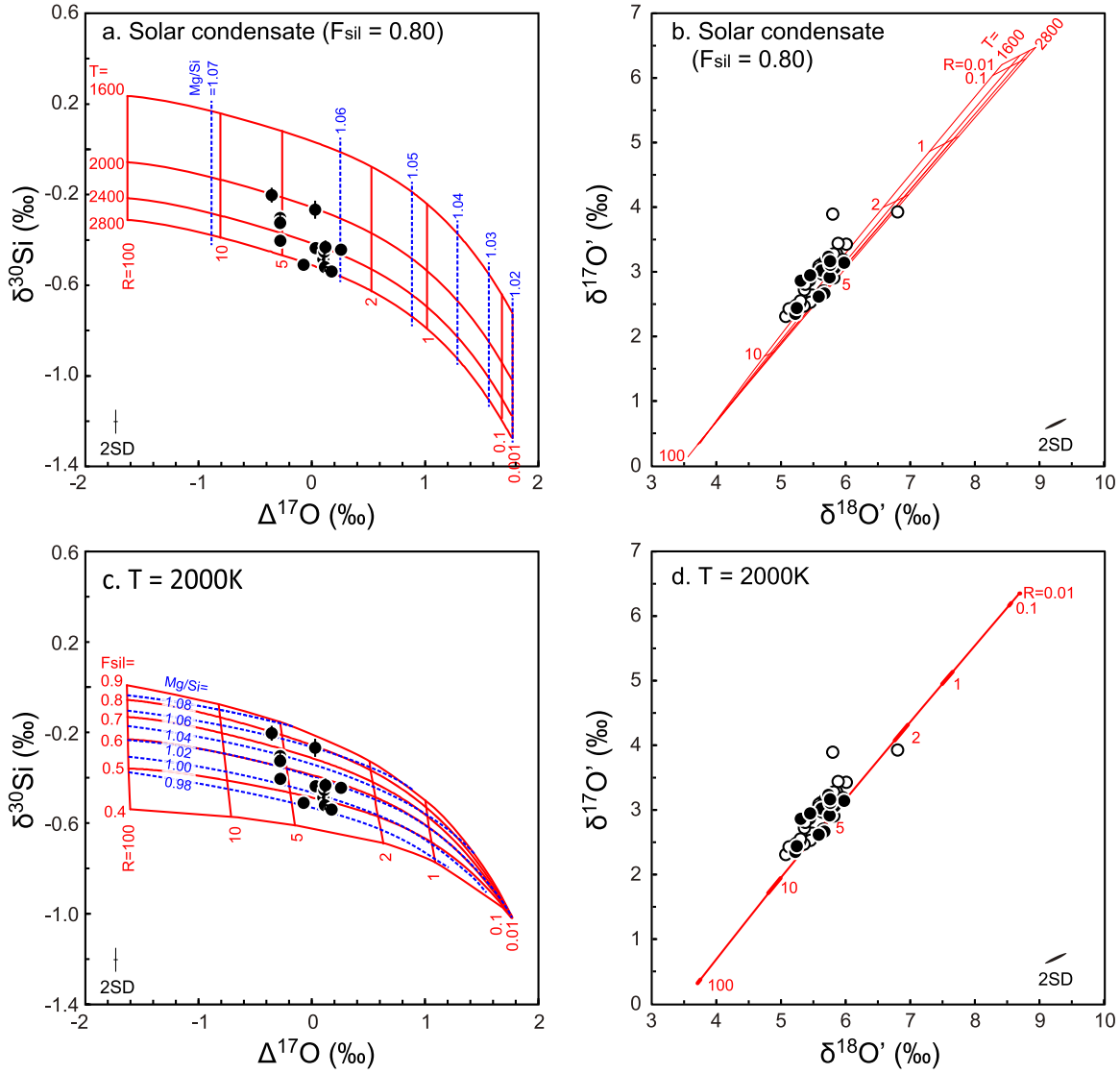

Figure 5. Calculated O and Si isotopic compositions of pyroxene using the model of evaporation-driven melt-gas interaction (red curves). Solid circles are the O and Si isotopic compositions of the EH3 and EH4 chondrules presented in Table 1. Open circles in panels b and d are the O isotopic compositions of EH3 and EH4 chondrules and enstatite separates (Tanaka & Nakamura 2017) whose Si isotopic compositions were not measured. Blue broken lines are Mg/Si atomic ratios of the dust-gas mixture. Panels a and b: Solar condensates (Fedkin & Grossman 2016) were used as the fixed dust composition ($F_{sil} = 0.80$) at variable T and R values. The proportion of silicate (including oxide), metal, and sulfide for solar condensates (Fedkin & Grossman 2016) is 0.63, 0.16, and 0.21 in weight by assuming that metal contains 3 wt.% of Si. Sulfide dust was not considered for the calculation because Si and O are absent in sulfide phases. Thus, the actual dust/gas ratio is 1.3 times higher than the R value. Panels c and d: The calculation was performed at $T = 2000$ K at variable F_{sil} values. The O and Si isotopic compositions of silicate and metal dust compositions were the same as were used for panels a and b.

by a melt-gas interaction process within a relatively low R and F_{sil} environment.

4.6. Implications for the Si and O Isotope Systematics of Inner Planetary Bodies

The total mass of the terrestrial planets and asteroids is 1.19×10^{25} kg, of which 51 wt.% is in the Earth–Moon system. Based on the estimated chemical compositions of the terrestrial planetary bodies (Trønnes et al. 2019), the Earth–Moon system accounts for 50% and 49% of the total O and Si contents, respectively, of the current inner planetary bodies. Due to the indistinguishable isotope systematics of O and many nucleosynthetic isotopes between ECs, BSE, and the Moon, it has been suggested that the major building blocks that formed the Earth–Moon and EC parent bodies originated from the same reservoir in the inner protoplanetary disk (Javoy et al. 2012; Dauphas 2017). However, the different Si isotopic compositions and Mg/Si ratios of ECs and BSE-Moon have made it difficult to explain the EC reservoir model for the Earth's formation (Javoy et al. 2012; Dauphas et al. 2015). The $\Delta^{17}O$ and $\delta^{30}Si$ values of the BSE-Moon are within the range of EC chondrules (Figures 1 and 3). Moreover, the Si and O isotopic compositions of most of the NC group differentiated planetary bodies (HEDs, angrites, Moon, Mars, and brachinite-like achondrites) are also identical with the range of these isotopes from EC chondrules. This result implies that the EC chondrules inherit the Si and O isotopic compositions of the precursor materials that formed the NC group differentiated planetary bodies.

The higher $\delta^{30}Si$ value for BSE relative to the chondritic value and ECs was inferred by Si fractionation between the Earth's metallic core and silicate mantle (Georg et al. 2007; Fitoussi et al. 2009; Armytage et al. 2011). To explain the Si

isotopic compositions of BSE by core-mantle fractionation from the EC reservoir, 20 to 30 wt.% of Si is necessary in the Earth's core, which is an unrealistic value (Fitoussi & Bourdon 2012; Sikdar & Rai 2020). From the carbonaceous or ordinary chondrite reservoirs, the Si isotopic composition of BSE can be explained by core-mantle fractionation with a reasonable Si mass fraction in the core (∼5 to 11 wt.%)(Savage et al. 2014). However, the O and nucleosynthetic isotopic compositions of the BSE cannot be explained by any fractionation process from the carbonaceous or ordinary chondrite reservoirs. The cause of heavy Si isotopic compositions of angrites also cannot be explained by core-mantle fractionation from any chondrite reservoirs (Dauphas et al. 2015). These arguments inferred that core-mantle fractionation could not generate the heavy Si isotope enrichment observed in BSE and angrites.

Other planetary processes, such as impact-induced volatile loss during accretion of planetesimals (Pringle et al. 2014) or a giant impact (Zambardi et al. 2013), or vapor loss from the melting of planetary bodies (Hin et al. 2017; Young et al. 2019) may be able to explain the elevated δ^{30}Si values of BSE, the Moon, and angrites. The depletion of the mass fraction of volatile elements, such as K, Rb, and Zn and the heavy isotope enrichment in these elements in the planetary bodies are more sensitive at tracing the volatile loss during planetary or nebular processes than Si (Paniello et al. 2012; Pringle & Moynier 2017; Tian et al. 2019). Depletion of K and Rb and their heavy isotope enrichments were observed in HEDs relative to ECs, Mars (analyzed only for K), and BSE, which could have been caused by extensive volatile loss during either planetary or nebular processes (Paniello et al. 2012; Pringle & Moynier 2017; Tian et al. 2019). Therefore the enrichment of heavy Si in the BSE cannot be explained by the higher degree of volatile loss relative to other NC group differentiated planetary bodies. These kinetic isotope fractionation processes cannot explain the cause of the variation in Δ^{17}O values either.

Our proposed model suggests that the dust-gas mixture in the EC chondrule-forming region should have higher Mg/Si at a higher R and $F_{\rm sil}$ condition (Figure 5(c)). If the major precursor materials of the inner planetary bodies were formed in the same region as the EC chondrules, the order of bulk Mg/Si of the nebular dust-gas mixture was Earth–Moon ≈ angrite >HED ≈ brachinite ≈ Mars >aubrite (Figures 3 and 5(c)). Dauphas et al. (2015) explained that the bulk Mg/Si of planetary bodies was controlled by isotopic equilibration between SiO gas and forsterite in the solar nebular, resulting in the proportional relationship for planetary bulk Mg/Si and δ^{30}Si. However, the model of Dauphas et al. (2015) did not consider the variation in O isotopic compositions of the examined planetary bodies. Our study demonstrates that the Mg/Si and Si and O isotopic compositions of the inner planetary bodies could be controlled by the degree of fractionation between the silicate and metallic dust of the solar condensate and the nebular reservoir's dust-gas ratio where EC chondrules were formed.

5. Conclusions

In this study, the relationship between high-precision O and Si isotopic data was presented for EC chondrules and ureilite. As a result, the following conclusions were reached:

(1) The chondrules in the least equilibrated enstatite chondrites (EH3 and EH4) possess a wide range in δ^{30}Si values that show a relationship with their corresponding Δ^{17}O values. With one exception, the δ^{30}Si values of EC chondrules at $\Delta^{17}O > -0.1‰$ are between −0.43‰ and −0.54‰, which are identical to the chondritic value (i.e., the value of carbonaceous and ordinary chondrites), while those with $\Delta^{17}O < -0.2‰$ are between −0.20‰ and −0.40‰, which are higher than that of the chondritic value. This relationship cannot be explained by equilibrium or kinetic isotopic fractionations, such as metal-silicate fractionation or vaporization processes.

(2) While the monomict ureilites measured in this study record a wide range of Δ^{17}O values, between −2.18‰ to −0.32‰, their δ^{30}Si values give a homogeneous value of $-0.45 \pm 0.06‰$ (2SD, $N = 15$), i.e., the 2SD value is comparable with that of the reference materials. The δ^{30}Si values of ureilites are identical with the chondritic value, suggesting that the rocky materials were homogenized in Si isotopic composition in the early (<0.1 Myr after the formation of the solar system) protoplanetary disk.

(3) The evolution of the δ^{30}Si value of the inner solar system could have proceeded as follows: The δ^{30}Si value of SiO in the solar nebula was initially low at ∼−7‰ when the AOA (Δ^{17}O ∼−25‰ to −20‰) and Fe-rich metal condensed. Subsequently, the δ^{30}Si values became higher, mainly due to metal condensation, and reached ∼2.5‰ by the time when the olivine-rich chondrule (Δ^{17}O ∼−6‰ to −1‰) and precursors of the ureilite parent body (Δ^{17}O ∼−2‰ to 0‰) were formed. Then, evaporation-driven melt-gas interactions between the forsterite-rich chondrule melts and the SiO-rich nebular gas that evolved by dust evaporation led to variations in the δ^{30}Si (−0.5‰ to −0.2‰) and Δ^{17}O (−0.5‰ to +0.8‰) values for enstatite-rich chondrules. The environment in which the EC chondrules formed had regions with relatively high and low dust/gas, silicate/metal in the dust, and Mg/Si in the dust-gas mixtures, which may have determined the variations in EC chondrules, with lower Δ^{17}O and higher δ^{30}Si and with higher Δ^{17}O and lower δ^{30}Si, respectively.

(4) The range in δ^{30}Si and Δ^{17}O values of the EH3 and EH4 chondrules overlaps with the values of the NC group differentiated planetary bodies. This indicates that their precursors' isotopic composition determined the O–Si isotopic compositions of these NC group differentiated planetary bodies. The Mg/Si of the dust/gas mixtures increases with increasing dust/gas ratio and silicate/metal ratio in the dust. The order of Mg/Si for the dust/gas mixture in the region where the major precursors of the inner planetary bodies were formed is estimated to be Earth–Moon ≈ angrite >HED ≈ brachinite ≈ Mars >aubrite.

The authors are grateful to T. Kunihiro and T. Ota for their constructive discussions, M. Ledevin, M. Yamanaka, C. Sakaguchi, and K. Tanaka for their technical help, and to D. Rumble and R.M.G. Armytage for their comments that improved the manuscript. The authors also acknowledge constructive reviews from three anonymous referees. We thank the National Institute of Polar Research, the Natural History Museum of Vienna, and the Royal Ontario Museum for loaning the meteorites. Financial support for this project was provided by the Program for Promoting the Enhancement of Research University by MEXT and by JSPS KAKENHI grants (20K04108).

ORCID iDs

Ryoji Tanaka https://orcid.org/0000-0002-7537-255X

References

Alexander, C. M. O. D., Grossman, J. N., Ebel, D. S., & Ciesla, F. J. 2008, Sci, 320, 1617
Ali, A., Jabeen, I., Gregory, D., Verish, R., & Banerjee, N. R. 2016, M&PS, 51, 981
Armytage, R. M. G., Georg, R. B., Savage, P. S., Williams, H. M., & Halliday, A. N. 2011, GeCoA, 75, 3662
Armytage, R. M. G., Georg, R. B., Williams, H. M., & Halliday, A. N. 2012, GeCoA, 77, 504
Béjina, F., & Jaoul, O. 1996, PEPI, 97, 145
Berthet, S., Malavergne, V., & Righter, K. 2009, GeCoA, 73, 6402
Budde, G., Burkhardt, C., Brennecka, G. A., et al. 2016, E&PSL, 454, 293
Clayton, R. N. 2002, Natur, 415, 860
Clayton, R. N., Hinton, R. W., Davis, A. M., et al. 1988, RSPTA, 325, 483
Clayton, R. N., & Mayeda, T. K. 1988, GeCoA, 52, 1313
Clayton, R. N., & Mayeda, T. K. 1996, GeCoA, 60, 1999
Clayton, R. N., Mayeda, T. K., Goswami, J. N., & Olsen, E. J. 1991, GeCoA, 55, 2317
Clayton, R. N., Onuma, N., Grossman, L., & Mayeda, T. K. 1983, in Chondrules and Their Origins, ed. E. A. King (Houston, TX: Lunar and Planetary Institute), 37
Dauphas, N. 2017, Natur, 541, 521
Dauphas, N., Poitrasson, F., Burkhardt, C., Kobayashi, H., & Kurosawa, K. 2015, E&PSL, 427, 236
Dauphas, N., & Schauble, E. A. 2016, AREPS, 44, 709
Davis, A. M., & Richter, F. M. 2014, TrGeo, 1, 335
Defouilloy, C., Cartigny, P., Assayag, N., Moynier, F., & Barrat, J. A. 2016, GeCoA, 172, 393
Fedkin, A. V., & Grossman, L. 2016, M&PS, 51, 843
Fitoussi, C., & Bourdon, B. 2012, Sci, 335, 1477
Fitoussi, C., Bourdon, B., Kleine, T., Oberli, F., & Reynolds, B. C. 2009, E&PSL, 287, 77
Fitoussi, C., Bourdon, B., & Wang, X. 2016, E&PSL, 434, 151
Franchi, I. A., Wright, I. P., Sexton, A. S., & Pillinger, C. T. 1999, M&PS, 34, 657
Georg, R. B., Halliday, A. N., Schauble, E. A., & Reynolds, B. C. 2007, Natur, 447, 1102
Georg, R. B., Reynolds, B. C., Frank, M., & Halliday, A. N. 2006, ChGeo, 235, 95
Greenwood, R. C., Burbine, T. H., Miller, M. F., & Franchi, I. A. 2017, ChEG, 77, 1
Greenwood, R. C., Franchi, I. A., Gibson, J. M., & Benedix, G. K. 2012, GeCoA, 94, 146
Grossman, L., Beckett, J. R., Fedkin, A. V., Simon, S. B., & Ciesla, F. J. 2008, RvMG, 68, 93
Hewins, R. H., & Connolly, J. 1996, in Chondrules and the Protoplanetary Disk, ed. R. H. Hewins, R. H. Jones, & E. R. D. Scott (Cambridge: Cambridge Univ. Press), 197
Hin, R. C., Coath, C. D., Carter, P. J., et al. 2017, Natur, 549, 511
Jacquet, E., Piani, L., & Weisberg, M. K. 2018, in Chondrules: Records of Protoplanetary Disk Processes, ed. H. C. Russell, Jr. & A. Krot (Cambridge: Cambridge Univ. Press), 175
Javoy, M., Balan, E., Méheut, M., Blanchard, M., & Lazzeri, M. 2012, E&PSL, 319, 118
Johansen, A., Mac Low, M.-.M., Lacerda, P., & Bizzarro, M. 2015, SciA, 1, e1500109
Kadlag, Y., Tatzel, M., Frick, D. A., & Becker, H. 2019, GeCoA, 267, 300
Kimura, M. 1988, in Proc NIPR Twelfth Symp. on Antarct Meteorites (Tokyo: National Inst. of Polar Research), 51
Kleine, T., Budde, G., Burkhardt, C., et al. 2020, SSRv, 216, 55
Krot, A. N., Nagashima, K., Lyons, J. R., Lee, J.-E., & Bizzarro, M. 2020, SciA, 6, eaay2724
Krot, A. N., Petaev, M. I., Russell, S. S., et al. 2004, ChEG, 64, 185
Lehner, S. W., Petaev, M. I., Zolotov, M. Y., & Buseck, P. R. 2013, GeCoA, 101, 34
Libourel, G., Krot, A. N., & Tissandier, L. 2006, E&PSL, 251, 232
Lodders, K. 2003, ApJ, 591, 1220
Marrocchi, Y., & Chaussidon, M. 2015, E&PSL, 430, 308
Marrocchi, Y., Villeneuve, J., Jacquet, E., Piralla, M., & Chaussidon, M. 2019, PNAS, 116, 23461
Martins, R., Chaussidon, M., Deng, Z., Pignatale, F., & Moynier, F. 2021, E&PSL, 554, 116678
Martins, Z., Chan, Q. H. S., Bonal, L., King, A., & Yabuta, H. 2020, SSRv, 216, 54
Martins, Z., Hofmann, B. A., Gnos, E., et al. 2007, M&PS, 42, 1581
Meheut, M., & Schauble, E. A. 2014, GeCoA, 134, 137
Newton, J., Franchi, I. A., & Pillinger, C. T. 2000, M&PS, 35, 689
Pack, A., Tanaka, R., Hering, M., et al. 2016, RCMS, 30, 1495
Palme, H., Hezel, D. C., & Ebel, D. S. 2015, E&PSL, 411, 11
Paniello, R. C., Moynier, F., Beck, P., et al. 2012, GeCoA, 86, 76
Patzer, A., & Schultz, L. 2001, M&PS, 36, 947
Piani, L., Marrocchi, Y., Libourel, G., & Tissandier, L. 2016, GeCoA, 195, 84
Pringle, E. A., & Moynier, F. 2017, E&PSL, 473, 62
Pringle, E. A., Moynier, F., Savage, P. S., Badro, J., & Barrat, J.-A. 2014, PNAS, 111, 17029
Pringle, E. A., Savage, P. S., Badro, J., Barrat, J.-A., & Moynier, F. 2013a, E&PSL, 373, 75
Pringle, E. A., Savage, P. S., Jackson, M. G., Barrat, J.-A., & Moynier, F. 2013b, ApJ, 779, 123
Prinn, R. G. 1993, in Protostars and Planets III, ed. E. H. Levy & J. I. Lunine (Tucson, AZ: Univ. Arizona Pres), 1005
Reynolds, B. C., Aggarwal, J., Andre, L., et al. 2007, JAAS, 22, 561
Rubin, A. E., Griset, C. D., Choi, B.-G., & Wasson, J. T. 2009, M&PS, 44, 589
Rubin, A. E., Wasson, J. T., Clayton, R. N., & Mayeda, T. K. 1990, E&PSL, 96, 247
Russell, S. D. J., Longstaffe, F. J., King, P. L., & Larson, T. E. 2010, GeCoA, 74, 2484
Sanders, I. S., Scott, E. R. D., & Delaney, J. S. 2017, M&PS, 52, 690
Savage, P. S., Armytage, R. M. G., Georg, R. B., & Halliday, A. N. 2014, Litho, 190, 500
Savage, P. S., Georg, R. B., Armytage, R. M. G., Williams, H. M., & Halliday, A. N. 2010, E&PSL, 295, 139
Savage, P. S., & Moynier, F. 2013, E&PSL, 361, 487
Schiller, M., Bizzarro, M., & Fernandes, V. A. 2018, Natur, 555, 507
Scott, E. R. D., & Krot, A. N. 2014, TrGeo, 1, 65
Scott, E. R. D., Taylor, G. J., & Keil, K. 1993, GeoRL, 20, 415
Sikdar, J., & Rai, V. K. 2020, NatSR, 10, 1273
Simon, S. B., Sutton, S. R., & Grossman, L. 2016, GeCoA, 189, 377
Tanaka, R., & Nakamura, E. 2013, RCMS, 27, 285
Tanaka, R., & Nakamura, E. 2017, NatAs, 1, 0137
Tian, Z., Chen, H., Fegley, B., et al. 2019, GeCoA, 266, 611
Trinquier, A., Birck, J.-L., & Allègre, C., Jr. 2007, ApJ, 655, 1179
Trinquier, A., Elliott, T., Ulfbeck, D., et al. 2009, Sci, 324, 374
Trønnes, R. G., Baron, M. A., Eigenmann, K. R., et al. 2019, Tectp, 760, 165
Valkiers, S., Ding, T., Inkret, M., Ruße, K., & Taylor, P. 2005, IJMSp, 242, 319
van Kooten, E. M. M. E., Wielandt, D., Schiller, M., et al. 2016, PNAS, 113, 2011
Villeneuve, J., Marrocchi, Y., & Jacquet, E. 2020, E&PSL, 542, 116318
Warren, P. H. 2011, E&PSL, 311, 93
Weisberg, M. K., & Kimura, M. 2012, ChEG, 72, 101
Weisberg, M. K., Prinz, M., & Fogel, R. A. 1994, Metic, 29, 362
Wiechert, U. H., Halliday, A. N., Palme, H., & Rumble, D. 2004, E&PSL, 221, 373
Williams, D. R. 2016, Planetary Fact Sheets (Greenbelt, MD: NASA), https://nssdc.gsfc.nasa.gov/planetary/factsheet/
Yin, Q.-Z., Yamashita, K., Yamakawa, A., et al. 2009, LPSC, 40, 2006
Young, E. D., Shahar, A., Nimmo, F., et al. 2019, Icar, 323, 1
Zambardi, T., Poitrasson, F., Corgne, A., et al. 2013, GeCoA, 121, 67
Ziegler, K., Chadwick, O. A., Brzezinski, M. A., & Kelly, E. F. 2005, GeCoA, 69, 4597
Ziegler, K., Young, E. D., Schauble, E. A., & Wasson, J. T. 2010, E&PSL, 295, 487